# Development of a background-oriented schlieren technique with telecentric lenses for supersonic flow

**F Cozzi[1], E Göttlich[3], L Angelucci[2], V Dossena[1] and A Guardone[2]**

[1]Politecnico Milano, Dipartimento di Energia, Via Lambruschini 4, 20156 Milano, Italy
[2]Politecnico di Milano, Dipartimento di Scienze e Tecnologie Aerospaziali, Via Lambruschini 4, 20156 Milano, Italy
[3]Graz University of Technology, Institute for Thermal Turbomachinery and Machine Dynamics, Inffeldgasse 25/A, 8010 Graz, Austria

E-mail: fabio.cozzi@polimi.it

**Abstract**. Background oriented schlieren (BOS) is a quantitative optical technique which exploits light deflection occurring in non-homogeneous transparent media. It allows to indirectly measure the density gradients by analysing the apparent displacement of features of a background pattern when imaged through the investigated flow. Thanks to its simple set-up and to the consolidated data reduction technique based on cross-correlation algorithms the BOS technique has progressively attracted the interest of the researchers. In this work a BOS system using a telecentric lens system has been set up in order to improve measurement accuracy and to avoid 3D effects arising from using conventional entocentric lenses. The design of the telecentric lens system is reported along with an analysis of its performance in term of spatial resolution. Some preliminary tests on a supersonic flows are also reported.

## 1. Introduction

The background orientend schlieren (BOS) is a line of sight optical technique that allows quantitative density measurements in inhomogeneous transparent flow. While the technique dates back to the work of Hubert Schardin [1], modern applications of BOS exploiting digital images recording and processing were pioneered in the early 2000's [2]-[3]. Compared to schlieren and shadow techniques BOS is simpler to set-up and allows to get quantitative density data more easily [4]-[5]. The BOS technique exploits light ray deflection occurring in inhomogeneous transparent medium to measure density gradients. Light ray deflection is estimated by comparing the images of a background pattern taken with and without the schlieren object (i.e. an inhomogeneous density field) in between the camera and the pattern. The Gladstone-Dale relationship between refractive index and density allows to retrieve density gradients from the measured displacements.

The popularity of BOS has grown rapidly in the last ten years also thanks to the continuous improving in image acquisition and analysis [6]. The BOS technique has been applied to investigate a wide spectra of phenomena: supersonic flows [4]-[7], rotor blade tip vortex of a full scale helicopter [8], free flight experiment [9], heat transfer in natural convection [10] and free jet [11] to name just but a few. Stereoscopic BOS configurations were used for the localization of a wing-tip vortex in a transonic wind tunnel [12], while tomographic approach have been also applied to single or

multicamera BOS set-up to reconstruct the 3D density fields [13]-[14]. The use of natural background for large scale outdoor BOS system have been also analyzed by Hargather and Settles [15]. A more comprehensive overview on applications of the BOS technique can be found in Raffel [6].

Imaging in BOS systems is usually accomplished by using entocentric lenses. The main feature of such lenses is to realize a central projection of the object plane (the subject) into the image plane (the camera sensor); chief rays in entocentric lenses are inclined respect the optical axis and image magnification depends upon object position even within the region of sharp imaging (i.e. the depth of field). Diverging light recording hinder the evaluation of the fluid density mainly for two reasons: firstly, light rays experience a variation in the gradient of the refractive index along their way through the schlieren object; secondly, the location at which ray displacement is measured differs from the location in the schlieren object that generated it. Thus even in plane 2D flows the diverging light recording can add uncertainty to the density gradient measurements.

Improvement in the quantitative application of BOS can be achieved by alleviating the previous issues through the use of telecentric lens. The main feature of such lens systems is that either its entrance pupil or its exit pupil is located at infinity [16],[17]. When both pupils are at infinity the system has an afocal configuration and it is called double side telecentric. The principal rays of a double side telecentric objective are parallel to the optical axis in both the image and the object space. Thus image originates by the parallel projection of the object onto the image plane and magnification is independent from the position of the object and the image planes. Telecentric systems offer also a quite wide depth of field being the aperture size usually quite small as compared to the focal length of the lenses. The most simple double side telecentric configuration is made by two positive lenses, separated by a length equal to the sum of their focal lengths, along with an aperture located at the common focal position of both lenses, see figure 1.

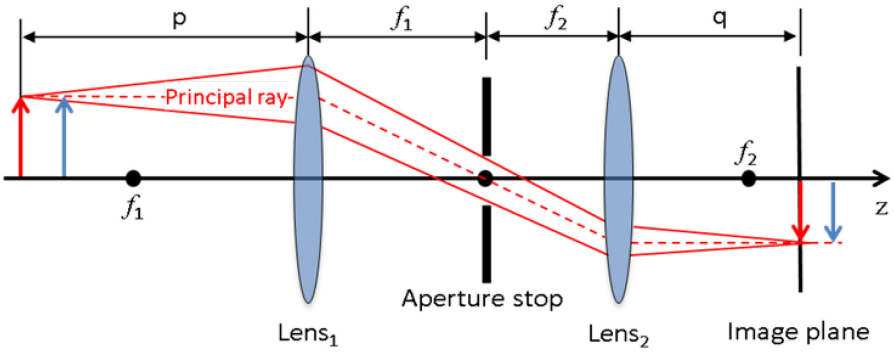


**Figure 1.** Double side telecentric lenses (afocal system).

When applied to BOS systems, double side telecentric objective is expected to offer some advantage: for plane 2D schlieren object being the imaging rays parallel to the optical axis they cross the density field along lines of constant density gradient, thus quantitative data can be obtained without the need of any correction or tomographic reconstruction. Moreover the location in the image at which the ray deflection is measured corresponds to the physical location at which the deflection is generated. Finally shadows cast by walls or obstacle are sharper if compared to entocentric lenses, thus measurements can be carried out at closer distance. The main disadvantage of telecentric lenses is the need for a frontal lens of at least the same size of the field of view.

Telecentric lenses are commonly employed in metrological application, while just few applications to BOS and PIV systems are reported in the literature [4], [18], [16]. Elsinga et al. [4] used a schlieren system with a diaphragm in place of the knife to perform BOS measurements in a supersonic 2D flow, this optical configuration is akin to a telecentric system. They compared estimated densities and density gradients with those obtained with an entocentric lens system showing better quantitative results for the telecentric configuration.

Recently Ota [18] applied a double telecentric-colored grid background-oriented schlieren (CGBOS) systems to investigate the supersonic flow around both axysimmetric and asymmetric models. The results were compared to those obtained with an entocentric lens system showing some improvement in the measured displacement field.

In this work a telecentric lens system for a BOS system has been set up. The design of the telecentric lens system is reported along with an analysis of its performances. Preliminary tests on a supersonic flows in a plane 2D over-expanded nozzle are also reported and commented.

## 2. Principles of the background oriented schlieren technique

Background oriented schlieren is an optical technique to measure density gradients within a transparent fluid. In optically transparent fluids the refractive index, $n$, is related to density, $\rho$, through the Gladston-Dale relation [19]:

$$n = 1 - G\rho \tag{1}$$

where $G$ is the so-called Gladstone-Dale constant. The Gladstone-Dale constant depends on both the nature of the propagation medium and the radiation wavelength, $\lambda$. Furthermore, equation (1) contains implicitly temperature and pressure that can be put in evidence by knowing the equation of state $\rho = \rho(T, p)$. According to equation (1) any density gradient gives rise to refractive index gradient and eventually to light rays deflection [17]. Thus details of a background object show an apparent displacement when seen through an inhomogeneous density field. By comparing the images of the background taken with and without the schlieren object the local image displacement $(\Delta x, \Delta y)$ can be measured. Displacements are converted to refractive index gradients by analyzing the ray path and finally to density gradients through equation (1). Advanced cross-correlation techniques commonly used in PIV measurements [11], or even optical flow algorithms [20], can be used to evaluate the displacement vector $\Delta\vec{r}(x, y) = (\Delta x, \Delta y)$ from BOS images.

A simplified scheme of a BOS setup is reported in figure 2. It is composed by a digital camera, imaging lenses, a background object and a lighting system. The background object usually is a random dot pattern on a surface behind the schlieren object. The pattern preferably has to have the highest spatial frequency that can be imaged with sufficient contrast.

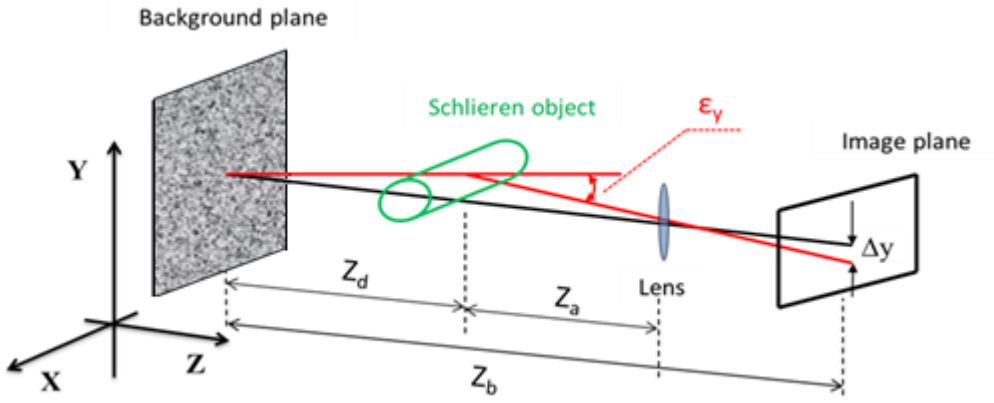


**Figure 2.** Sketch of a BOS optical setup.

For paraxial recording and small deflection angles ($\varepsilon_y \approx \tan \varepsilon_y$), the apparent image displacement $\Delta y$ along the $y$ direction is proportional to the deflection angle $\varepsilon_y$ [21], figure 2:

$$\Delta y = M Z_d \varepsilon_y \tag{2}$$

where $Z_d$ is distance between the background and the plane at which the light ray deflection can be assumed to have fully occurred and $M = (Z_b - Z_d - Z_a)/(Z_d + Z_a)$ is the magnification of the

entocentric lens system. $Z_a$ is the schlieren object to lens distance and $Z_b$ is the background plane to image plane distance. Equation (2) holds also for telecentric lens system provided the magnification $M$ is that given by equation (6) [18]. The sensitivity $S$ of the BOS system is defined as $S = \Delta y/\varepsilon_y = MZ_d$. The deflection angle $\varepsilon_y$ and the refractive index gradient along the $y$ direction, $\partial n/\partial y$, are linked through equation (3) [22].

$$\varepsilon_y(X_s, Y_s) = \int_{Z_s}^{Z_s+W} \frac{1}{n}\frac{\partial n}{\partial y} dz \tag{3}$$

where $W$ is the width of the schlieren object and $X_s, Y_s$ and $Z_s$ are the entrance coordinate of the light ray in the schlieren region. According to equation (1) and equation (3) the deflection angles $\varepsilon_y$ results to be a linear function of $\partial\rho/\partial y$ in plane 2D density fields, see equation (4),

$$\varepsilon_y(X_s, Y_s) \cong \frac{G}{n_0} W \frac{\partial \rho}{\partial y} \tag{4}$$

where $n_0$ is the refractive index of the fluid at $(X_s, Y_s, Z_s)$. A similar relationship also holds for displacements and deflection angles along the $x$ direction, thus the density gradient $\vec{\nabla}\rho = (\partial\rho/\partial x\,, \partial\rho/\partial y)$, can be estimated from the image displacement vector, $\Delta\vec{r}(x_s, y_s) = (\Delta x, \Delta y)$, through equation (5):

$$\vec{\nabla}\rho\left(X_s, Y_s, Z_s + \frac{W}{2}\right) \cong \frac{n_0}{W \cdot G \cdot M Z_d} \Delta\vec{r}(x_s, y_s) \tag{5}$$

where $(x_s, y_s)$ are the coordinates $(X_s, Y_s)$ projected into the image plane.

## 3. Telecentric lens design and testing

The telecentric systems is made of two positive thin lenses, having focal lenghts $f_1$ and $f_2$, separated by a distance equal to the sum of their focal distances. A diaphragm is located in the common focal point, see figure 1. The magnification of the telecentric lenses system, $M$, and the conjugate image and object distances $p$ and $q$ are given by equation (6) and equation (7), respectively [16].

$$M = \frac{f_2}{f_1} \tag{6}$$

$$q = f_2\left[\frac{f_2}{f_1}\left(1 - \frac{p}{f_1}\right) + 1\right] \tag{7}$$

For a real image to be formed on the camera sensor plane the image to lens distance should be positive, i.e. $q > 0$, thus equations (6) and (7) imply $p \leq f_1(1 + 1/M)$. For magnification not too far from unit a real image is formed at a distance $p$ of the order of $f_1$. Combining equation (6) and equation (2) the image displacements, $\Delta y$, results to be a linear function of ray deflections, $\varepsilon_y$, as per equation (8).

$$\Delta y = \frac{f_2}{f_1} Z_d \varepsilon_y \tag{8}$$

Differently from the entocentric system, $\Delta y$ is not affected by $Z_a$. According to Berger [23] when the object to lens distance $q$ is equal to $f_1$ magnification shows a minimum sensitivity to axial positioning errors of the optical elements. Thus the system was designed for coniugate distances $q = f_1$ and $p = f_2$.

The required lens magnification is set by the camera sensor size, $L_c$, and the physical field of view, $L_{FW}$ as per equation (9).

$$M = \frac{L_C}{L_{FW}} \tag{9}$$

In our case we use a CMOS camera having a square sensor of size $L_c$≅16.4 mm. Setting the field of view equal to the height of the exit section of the nozzle, i.e. $L_{FW}$ =30 mm, the magnification resulted to be about 0.55. The telecentric system was assembled by using two lenses available in the laboratory

and suitable for the required magnification. The lenses have focal lengths of $f_1$=310 mm and $f_2$=150 mm and diameters of about $D_{L1}$=80 mm and $D_{L2}$=51 mm, respectively. From equation (4) the nominal magnification resulted to be $M_{nom}$ = 0.484, this value is about 15% smaller than desired giving a slightly wider field view.

A suitable aperture has to be placed at the common focal point of the two lenses to get the telecentric optical system. The diameter of the aperture, $d$, besides setting the amount of light reaching the image plane, affects also the depth of field and the resolving power of the optical system. By decreasing $d$ the system became more tolerant to out of focus [23], while depth of field increases and resolving power decreases.

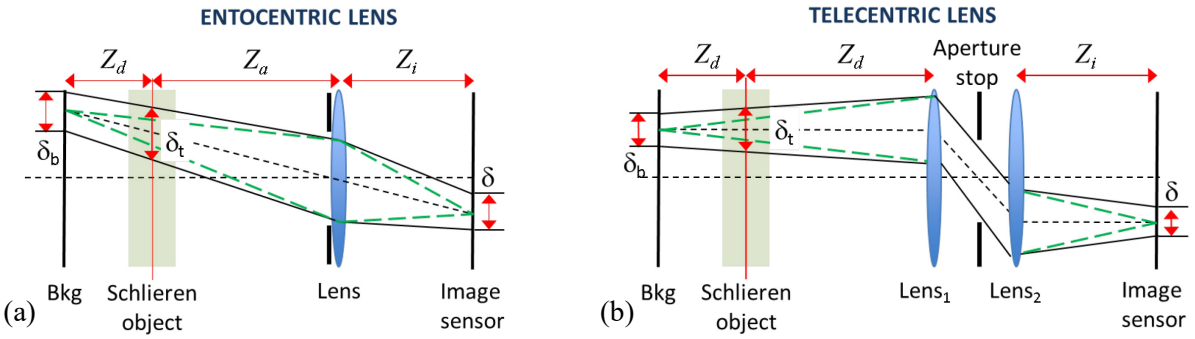


**Figure 3.** BOS setup for entocentric (a) and telecentric (b) optical systems, $\delta_b = \delta/M$ is the size of the circle of confusion projected back on the object plane.

The optimum size of $d$ is chosen by maximizing the spatial resolution, $\delta_t$, of the BOS measurement. The latter is the size of the schlieren region that contribute to the apparent displacement of the smallest resolvable feature of the background target, thus refractive index variation occurring in region smaller than $\delta_t$ cannot be resolved. Figure 3 shows the BOS setups for entocentric and telecentric optical systems along with their spatial resolution $\delta_t$. The analysis of $\delta_t$ for entocentric BOS system was examined by Klinge et al. [12] and by Gojani et al. [24], the analysis was later extended to telencentric system by Ota et al. [18]. As done in [24] and in [18] and differently from [12] the spatial resolution $\delta_t$ considered here do not take into account the size of the interrogation area used to estimate the apparent image displacement. Expression of $\delta_t$ for entocentric and telecentric systems are given in equations (10) and (11), respectively.

$$\delta_t = \frac{M}{M+1} Z_d \frac{d}{f} + \frac{\delta}{M}\left(1 - \frac{Z_d}{Z_d+Z_a}\right) \tag{10}$$

$$\delta_t = Z_d \frac{d}{f_1} + \frac{\delta}{M} \tag{11}$$

Where $\delta$ is the diameter of the circle of confusion. The first term on the RHS of both equations (10) and (11) is the diameter at the refractive plane of the light cone emitted from one point on the background, while the second one is the size of the confusion diameter projected onto the refractive plane. It has to be pointed out that lens aberrations are not taken into account, thus equations (10) and (11) are expected to underestimate the value of $\delta_t$.

The size of the circle of confusion depends on the size of the aperture that control the amount of light collected by the optical system [17],[25]. According to the Rayleigh criterion and for monochromatic light of wavelength λ, the diameter of the circle of confusion of a telecentric lens system is $\delta = 1.22\lambda f_2/d$ [25], by substituting $\delta$ in equation (11) we get for $\delta_t$ the expression in equation (12). The spatial resolution $\delta_t$ results to be a function of the aperture size $d$, while the focal length of the frontal lens, $f_1$, the distance $Z_d$ and the wavelength λ can be considered as fixed parameters.

$$\delta_t = Z_d \frac{d}{f_1} + \frac{1.22\,\lambda\, f_1}{d} \tag{12}$$

The function $\delta_t(d)$ is plotted in figure 4 for $f_1$=310 mm, λ=460 nm and $Z_d$ =30 mm, and it shows to have a minimum. The aperture size, $d_{opt}$, corresponding to that minimum is given by equation (13).

$$d_{opt} = \left(1.22 \frac{\lambda}{Z_d}\right)^{1/2} f_1 \tag{13}$$

For $d = d_{opt}$ the two terms in the LHS of equation (12) result to be equal and equation (14) gives the optimum spatial resolution, $\delta_{opt}$, of the telecentric BOS system.

$$\delta_{opt} = 2 * (1.22 \lambda Z_d)^{1/2} \tag{14}$$

It is interesting to note that while $d_{opt}$ is a linearly function of $f_1$, $\delta_{opt}$ does not depend on either $f_1$ or $f_2$. This means that for fixed $Z_d$ and λ, $f_1$ and $f_2$ can be freely chosen to adjust magnification without affecting $\delta_{opt}$. By using equation (13) $Z_d$ can be eliminated from equation (14) getting $\delta_{opt} = 2.44\,\lambda\, f_1 / d_{opt}$, thus optimum resolution and optimum aperture are inversely proportional.

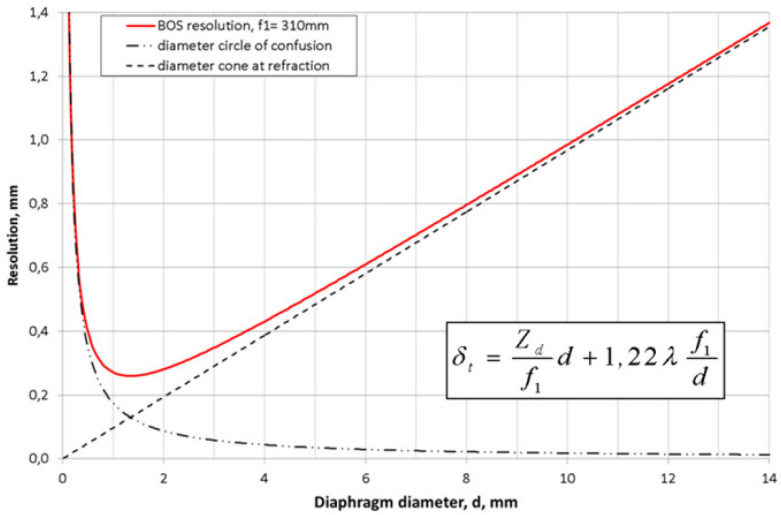


**Figure 4.** Continuous line: spatial resolution of telecentric BOS systems, $\delta_t$, computed from equation (12), $f_1$=310 mm, λ=460 nm and $Z_d$ =30 mm. Dashed lines are contribution to $\delta_t$ from the two single terms on the RHS of equation (12).

Figure 5 shows $d_{opt}$ and $\delta_{opt}$ computed through equation (13) and equation (14) for background to schlieren object distance, $Z_d$, varying between 0 and 100 mm, while $f_1$=310 mm, λ=460 nm and $Z_d + Z_a$ =300 mm are kept constant. Figure 5 evidence that $d_{opt}$ decreases and $\delta_{opt}$ increases as $Z_d$ increases; thus to improve resolution short background to schlieren object distance, $Z_d$, and wide aperture, $d$, are both required. Being the BOS sensitivity, $S$, decreasing when $Z_d$ decrease a trade-off is required between resolution and sensitivity.

The assembled telecentric objective attached to the CMOS camera is shown in figure 6. A manually variable iris is placed in the common focal point of the two lenses, this allows $d$ to be freely adjustable between 0.8 mm and 25 mm.

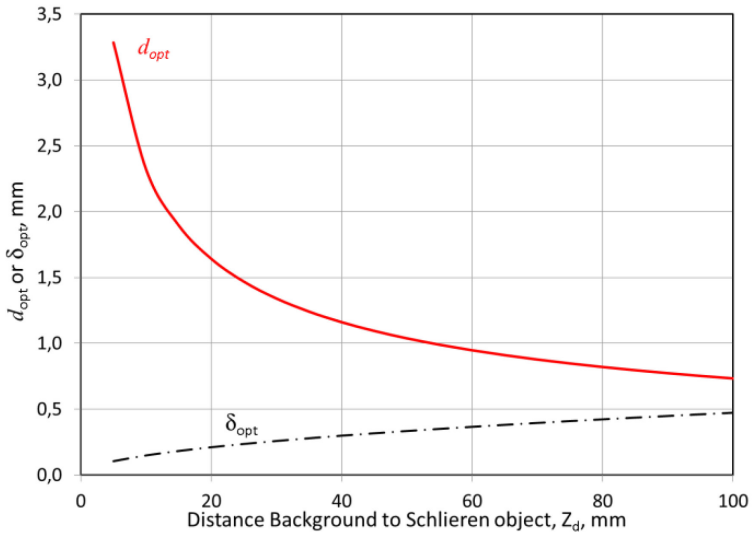


**Figure 5.** Optimum aperture size, $d_{opt}$, and optimum resolution $\delta_{opt}$ computed through equations (13) and (14) as a function $Z_d$ ($f_1$=310 mm and λ=460 nm).

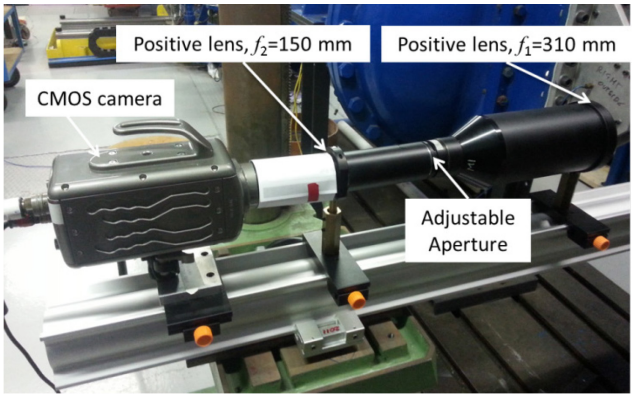


**Figure 6.** Photo of the telecentric lens systems mounted on the CMOS camera.

The actual magnification of a lens system depends on parameters that cannot be easily measured with good accuracy (i.e. actual position of lenses, their actual focal length etc.) thus calibration is required. The telecentric assembly was tested for magnification and for telecentric degree by imaging a printed calibration pattern (square grid 5 mm by side of circular dots) located at the focusing distance (i.e. 310 mm) and at +/-20 mm away from it (about +/- 6.5 % of $f_1$). For aperture sizes of 1, 2, and 7 mm, magnification $M$ resulted to be equal to 0.479, i.e. very close to the nominal value of 0.484; magnification changed of about +/- 0.2% over the out of focus rage of 40 mm. Depth of field was also roughly estimated by imaging a ruler 30° inclined respect to the optical axis. The depth of field resulted to be about 65 mm for both $d \cong 1$ mm and $d \cong 2$ mm, and it decreases to about 40 mm for $d \cong 7$ mm.

Based on previous results and on some preliminary tests with $Z_d = 30$ mm the diameter $d$=2 mm seemed to be the best choice for the diaphragm aperture. This aperture is twice the optimum one, see figure 4 and figure 5, nevertheless it improves light collections and gives sharper images, without significantly affecting the depth of field and telecentric degree.

To check system sensitivity, $S$, tests were performed with the telecentric BOS system using a positive thin lens having a focal length $f_{test}$=1000 mm as a schlieren object. The radial image displacement, $(\Delta x^2 + \Delta y^2)^{1/2}$, is a linear function of both radial distance, $r$, from the optical axis and sensitivity, as given by equation (15).

$$(\Delta x^2 + \Delta y^2)^{1/2} = S\,r/f_{test} \tag{15}$$

Two values of $Z_d$ were tested: 31.5 mm and 61 mm, for $M$=0.479 the nominal sensitivity $S = MZ_d$ resulted to be 15.1 and 29.5 mm/rad, respectively. The horizontal image displacement, $\Delta x$, along the horizontal axis is shown in figure 7(a), as expected it shows an almost perfect linear variation with $r$. A linear fit of the measured displacements allows to estimate a sensitivity of 15.2 mm/rad and of 29.5 mm/rad for $Z_d$=31.5 mm and $Z_d$= 61 mm, respectively, almost in perfect agreement with the nominal ones. The radial displacement over the whole test lens is shown in figure 7(b) and it evidences a very good axisymmetric distribution. The almost uniform zero-displacement region in the bottom of figure 7(b) is originated by the image of the lens support.

The measured performances evidence the proper design and assembly of the optical system.

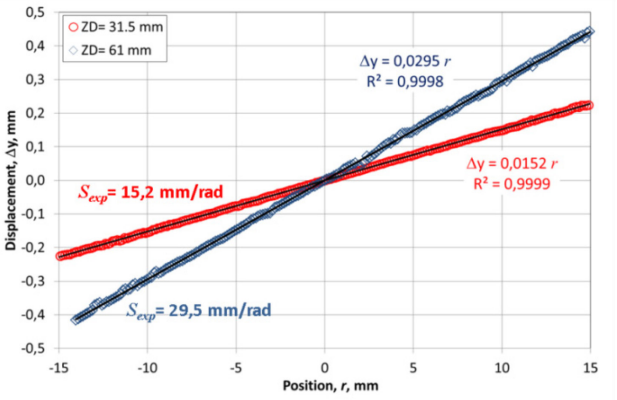


(a)

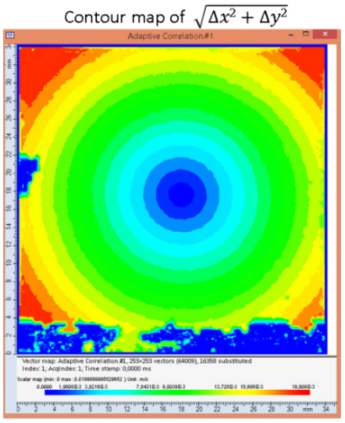


(b)

**Figure 7.** (a) Horizontal image displacement along the horizontal axis for $Z_d$= 31.5 mm and 61 mm. (b) Contour of radial displacement $(\Delta x^2 + \Delta y^2)^{1/2}$ for $Z_d$ = 61 mm.

## 4. Experimental set-up

To test the telecentric BOS system, the flow at the exit of an over-expanded convergent-divergent (CD) nozzle is investigated. Experiments are carried out in a supersonic 2D blow-down wind tunnel. A plane parallel-walled CD nozzle with a nominal area ratio $A_e/A_t$ =1.5 and 12.3 mm in width is attached to the plenum of the wind tunnel through a trumpet-shaped convergent section. The nozzle exit section has a height of about 30 mm. The plenum is a pressurized cylindrical vessel providing the stagnation condition for the flow, a piezoresistive pressure transducer with a full scale of 800 kPa (extended accuracy = 0.08% of the full scale) and a thermocouple probe (<1% accuracy) measure the stagnation pressure and temperature, respectively. Tests are carried out at total pressures of about 350 kPa and 500 kPa and at a constant total temperature of about 291 K (+/0.5 K). The nozzle discharges into ambient atmosphere where pressure is about 1 bar. Two plane BK7 8 mm thick glass windows (refractive index $n_{BK7} \cong 1.52$) provide the transparent side walls for the 2D CD nozzle. A photo of the experimental set-up is shown in figure 8.

Pressure measurements are taken at discrete position along the nozzle axis, pressure taps are located on a brass plate which is put in place of the rear glass window. Due to the brass plate, BOS and pressure measurements cannot not be carried out simultaneously. The plate has 17 pressure taps drilled along its axis of symmetry, taps are 0.5 mm in diameter and equally spaced under 5 mm. Each pressure tap is connected to piezoresistive pressure transducers through silicon pipes, the transducers have a full scale of 350 kPa their extend accuracy was 0.05 % of the full scale. A complete scan requires a few tens of seconds, for each test condition the scan is repeated 3 times. The three measurements series are averaged together and pressures vary of about 0.2 % from scan to scan.

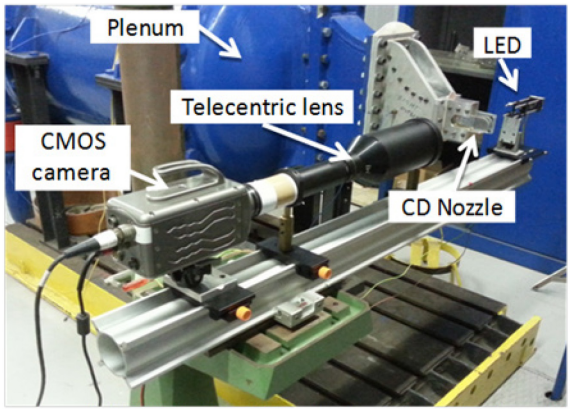


**Figure 8.** Experimental set-up.

The BOS system is composed by a CMOS camera, the telecentric lens system described above and a blue LED for lighting, see figure 8. The camera has a resolution of 1024*1024 pixels and a pixel pitch of 16 μm. The telecentric lens system uses an aperture size set to 2 mm for all the tests reported here. The lighting system is composed by a high power LED (Osram Ostar LE B Q9WN), emitting at a wavelength of 460 nm. The emitting surface has an area of 0.9*0.9 $mm^2$ and the LED operates at a constant current of about 700 mA corresponding to a nominal light output power of about 1 W. To improve light uniformity over the translucent target, the central portion of the light beam is expanded by means of a lens system. The recorded images show a spatially uniform and constant in time light intensity.

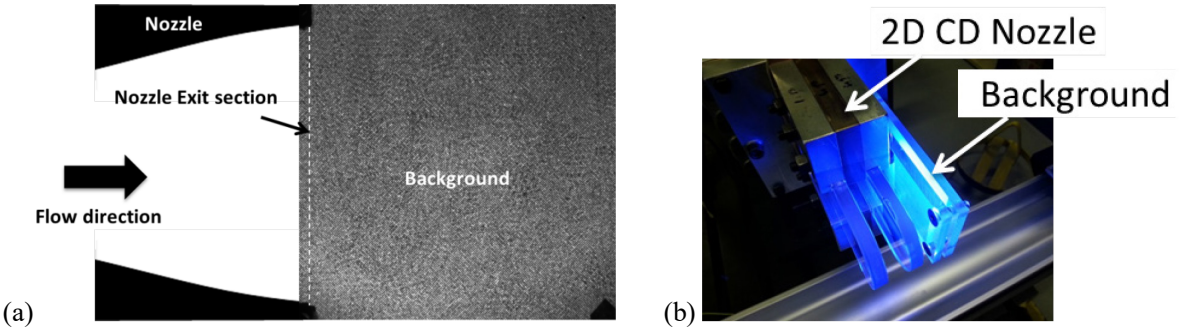


**Figure 9.** (a) Sample background image recorded by the BOS system, the sketch added to the left of the image shows flow direction and the shape of the diverging section of the nozzle. (b) Background pattern lightened by the LED.

The background is an artificially generated speckle pattern. The spatial distribution of the grey and white structures of the picture used as background is casual and generated using a Gabor noise. This particular type of noise, based on the Gabor's convolution, is particularly indicated for this kind of application because it permits a strict control of the spatial frequency of the generated pattern [26]. The image was printed on a transparent at resolution of 600 DPI (about 42 μm per printer dot) by using a laser printer and a sample background image is shown in figure 9(a). The speckle dots size, estimated from a visual inspection, resulted to be about 4 pixels, this value corresponds also to the width of the cross-correlation peak given by the PIV software. Such dot size is slightly big but still in the optimal range of 2-4 pixels suggested by Adrian [27]. Due to limitation in printer resolution, the speckle dots size couldn't be reduced and the printed image has a more or less regular pattern of small black and white dots with a spatial frequency of about 1/8 $pixels^{-1}$. The background target is placed between two PMMA plates, each 6 mm thick (refractive index $n_{PMMA} \cong 1.49$), and is firmly stuck to the nozzle structure at 30 mm distance from the rear window, see figure 9(b).

## 5. Analysis procedure of BOS images

This section provides a brief description on the technique used for analyzing BOS images. To evaluate the actual spatial position at which the ray displacement originates, the flow images are used as the references ones against which the undistorted background image is compared [4]. The virtual image displacement is estimated by applying an adaptive cross-correlation algorithm (3 steps) with a final interrogation area (IA) of 16 by 16 pixels and 75% overlap, the final mesh size in the object space is about 0.28 x 0.28 mm$^2$. The analysis is implemented using a commercial PIV software (DynamicStudio 4.15a by Dantec). No image pre-processing is implemented and a single couple of image is analyzed for each run.

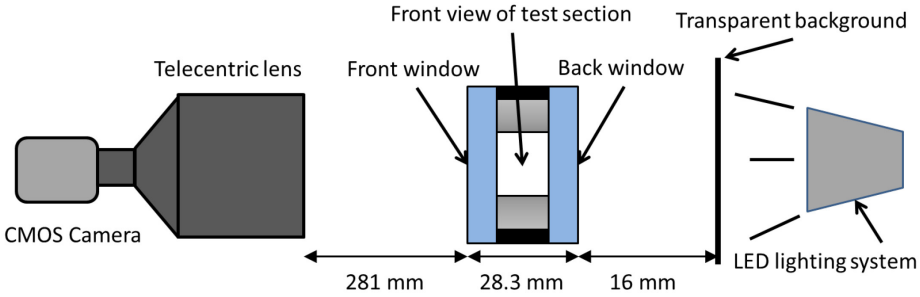


**Figure 10.** Side view of the telecentric BOS system, including test section (front view) and lighting system.

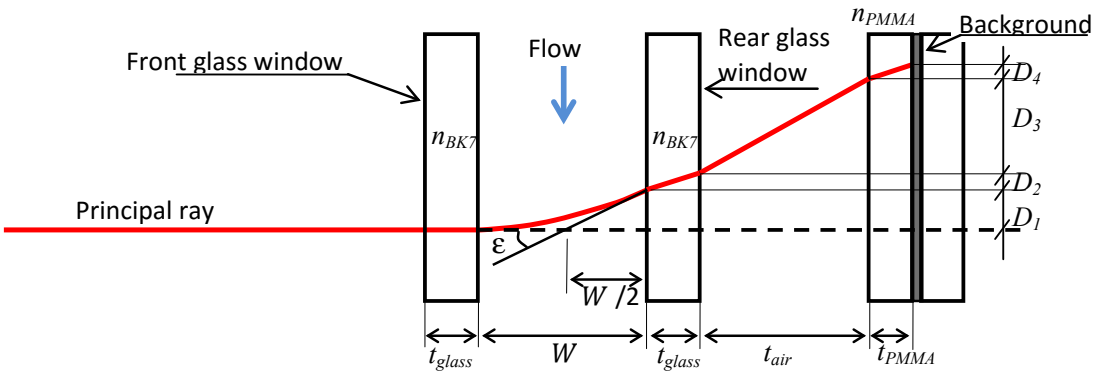


**Figure 11.** Top view of the test section (the nozzle is not shown) and of the principal ray (continuos thick line). The path of the principal ray in case of no refraction is shown as a dashed line.

In order to recover the angular deflection $\varepsilon_y$ from the measured displacement $\Delta y$, the schlieren object to background distance $Z_d$ has to be evaluated. Optical components distances are shown in figure 10, while a detailed view of the principal light ray path is shown in figure 11. The back glass window and the PMMA plate contribute to ray refraction, so they have to be taken into account to correctly estimate the angular deflection originated by the schlieren object. Moreover since the nozzle width is comparable to the distance between the background and the back window, it cannot be neglected. For a supersonic wind tunnel with thick windows Elsinga et al. estimated $Z_d$ by using a ray tracing procedure [4], anyhow due to the different optical set-up their results cannot be directly used here. The telecentric lens systems and its wide depth of field allows us to limit our analysis to the principal ray and on how it is refracted by the flow and by the interfaces it encounters along its way, figure 11. The total apparent displacement, $\Delta Y = \sum_i D_i = \Delta y / M$, in the background plane is given by the sum of the displacements occurring in each transparent medium, $D_i$, see figure 11. Being perpendicular to the principal ray the front window doesn't give any contribution to the total displacement and it is not taken into account. By summing all displacements and assuming small ray

deflection angles, i.e. $\varepsilon_y \cong \tan(\varepsilon_y)$, $\varepsilon_y$ is given by equation (16),

$$\varepsilon_y \cong \tan(\varepsilon_y) = \frac{\Delta y}{M}\left[\left(\frac{W}{2} + t_{air} + \frac{t_{glass}}{n_{BK7}} + \frac{t_{PMMA}}{n_{PMMA}}\right)^{-1}\right] \quad (16)$$

thus $Z_d$ is given by equation (17):

$$Z_d = \left(\frac{W}{2} + t_{air} + \frac{t_{glass}}{n_{BK7}} + \frac{t_{PMMA}}{n_{PMMA}}\right) \quad (17)$$

where $t_{air}$, $t_{glass}$ and $t_{PMMA}$ are the thicknesses of the different media shown in figure 11. If we assume that the background is stuck to the outside of the rear window (i.e. $t_{PMMA}$=0 and $t_{air} = 0$) equation (16) and equation (17) exactly recovers the ones obtained by Elsinga et al. [4].

Using $W$ =12.3 mm, $t_{air}$=16 mm, $t_{glass}$=8 mm and $t_{PMMA}$=6 mm, we get $Z_d$ = 31.4 mm, Without properly accounting for refractions, we would get $Z_d = \left(W/2 + t_{air} + t_{glass} + t_{PMMA}\right)$=36.2 mm, i.e. a value almost 15% higher than the correct one, thus angular deflections and density gradients would have been underestimated of almost the same percentage.

A source of error often neglected in BOS measurement is due to vibrations or channel movement occurring during the tests. The unwanted camera or wind tunnel movements add to the ones originated by the phase object and they act as a spurious displacement affecting the estimation of the density field [4]. A proper way to remove the bias is required if accurate density measurement are sought.

Neither density gradient nor density are evaluated in this work, thus bias from channel movement is not of concern, while equation (8) and equation (17) have not to be used. Anyhow due to their relevance for density estimations they have been reported and discussed.

## 6. Experimental Results

For a fixed nozzle geometry and working fluid, the flow field depends on the nozzle pressure ratio NPR (i.e. the ratio between reservoir total pressure $P_0$ and external pressure $p_e$) [28]. If NPR is equal to the design value ($NPR_d$), the static pressure at the nozzle exit is equal to ambient pressure and the flow inside the nozzle can be assumed iso-entropic. When NPR is greater than $NPR_d$ the nozzle is under-expanded, the exhaust pressure is greater than the outside ones and Prandtl-Mayer fans appear outside the nozzle. On the other hand, if NPR is smaller than $NPR_d$, the nozzle is over-expanded and some shock waves appear inside or outside the nozzle depending of the over-expansion level. The actual area ratio is difficult to be estimated accurately, thus actual $NPR_d$ is estimated as $P_0/p_s$ where $p_s$ is the static pressure measured at the nozzle exit section when neither shock waves nor flow separation occur in the nozzle. Assuming the exit section of the nozzle located approximately halfway between two pressure taps, $p_s$ is computed as the average of the values measured at those two taps. $NPR_d$ results to be about 5.36, while tests are conducted with NPR=5 and 3.5, thus the nozzle always operates in over-expanded conditions. Boundary layer thickness and uncertainty in the measurement of the area ratio $A_e/A_t$ prevent the accurate estimate of the exit Mach number, $M_{e,iso}$, directly from the latter. For iso-entropic nozzle flow, a more reliable estimate of $M_{e,iso}$ is obtained from pressure measurements by using equation (18),

$$M_{e,iso} = \left\{\frac{2}{\gamma-1}\left[\left(\frac{P_0}{p_s}\right)^{\frac{\gamma-1}{\gamma}} - 1\right]\right\}^{1/2} \quad (18)$$

where the ratio between the specific heats is γ=1.4. For all the tested conditions neither shock waves nor flow separation occurred inside the nozzle, thus iso-entropic flow condition can be assumed. By using equation (18) and the measured pressure ratios, $P_0/p_s \cong 0.187$, we get $M_{e,iso} \cong 1.75$. The exit Mach number estimated from the nominal area ratio, $A_e/A_t$ =1.5, is 1.85, i.e. about 6% higher than the actual one.

When NPR=5, the nozzle is over-expanded and two oblique shock waves appear outside the CD nozzle. The contour maps of horizontal, $\Delta x$, and vertical, $\Delta y$, displacements are shown in figure 12(a)

and 12(b), respectively. A bias of about 7-8 pixels due to wind tunnel/camera movement can be seen in the horizontal displacements, while a much smaller one, about 1 pixels, affects the vertical ones. The oblique lines seen in figures 12(a)-(b) are the traces of the shock waves originated in the upper and lower side of the nozzle by the over-expanded condition. It can be observed that a shock wave is composed by two closely spaced lines, the latter corresponds to regions where the measured displacement is either smaller or bigger than the ones due to the bias. Such behavior is likely due to limitation of the BOS technique in reproducing very sharp density variation and not to the flow, anyhow such issue is behind the scope of the present work and was not further investigated. The over-expansion level is weak enough for a simple reflection to occur where the two shocks waves intersect. The incidence angles of the original as well as of the reflected shocks and the inclination of the shear layer measured to the horizontal direction are marked as $\theta_1, \theta_2$ and $\delta$, respectively. They can be computed by means of oblique shock tables using the estimated $M_{e,iso}$, and experimentally measured by a visual analysis of the displacements maps. The computed angles are $\theta_1 \cong 36.7°, \theta_2 \cong 36.4°$ and $\delta \cong 2°$, resulting in very good agreement with the measured ones: $\theta_1^{exp} \cong 36°, \theta_2^{exp} \cong 36°$ and $\delta^{exp} \cong 2°$.

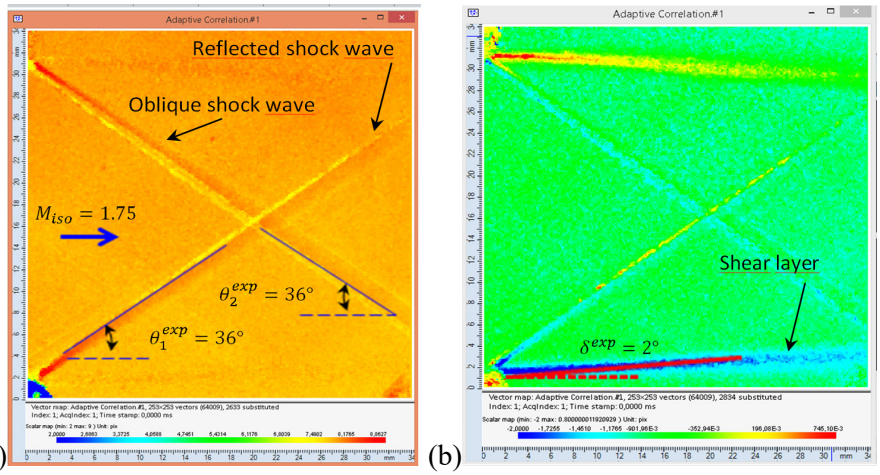


**Figure 12.** Displacements $\Delta x$ (a) and $\Delta y$ (b) in pixel for NPR=5 with $P_0$=350 kPa, $p_e$=100 kPa, $T_0$=294 K and $M_{e,iso}$=1.75.

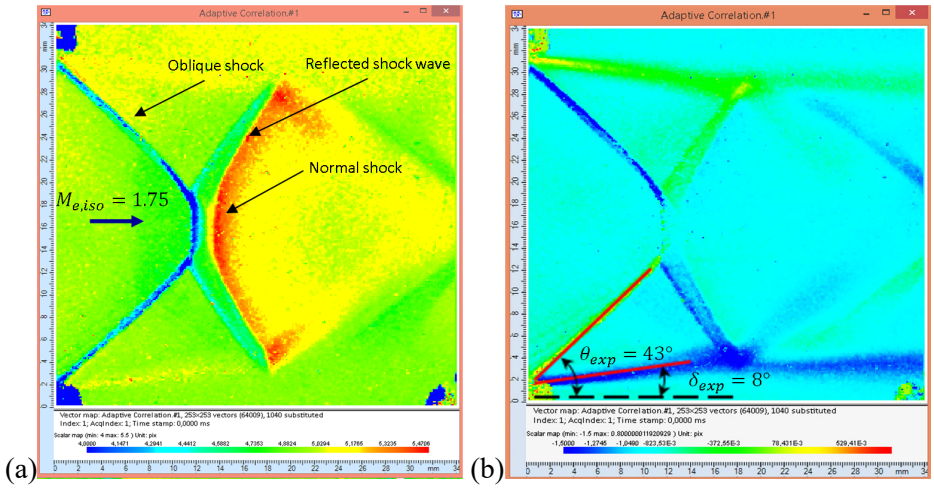


**Figure 13.** Displacements $\Delta x$ (a) and $\Delta y$ (b) in pixel for NPR=3.5 with $P_0$=350 kPa, $p_e$=100 kPa, $T_0$=294 K and $M_{e,iso}$=1.75.

As the NPR decreases the turning imposed to the flow by the oblique shock system increases and a simple shock reflection is no longer possible. As shown in figure 13 the BOS technique is able to catch the complex shock structure named Mach reflection appearing into the flow at NPR=3.5. Three main elements can be seen: an incident oblique shock, a reflected oblique shock and an almost normal shock generally known as Mach steam. The same procedures described above were used to evaluate the slopes of shocks and of the shear layer. The theoretical results are: $\theta_1 \cong 44.2°$, $\delta \cong 8.7°$, they are in good agreement with the measured angles, $\theta_1^{exp} \cong 43°$, $\delta^{exp} \cong 8°$. The above results evidence the capability of the telecentric BOS system to correctly identify shock structures in over-expanded nozzle flows.

## 7. Conclusions

In this work a BOS technique using a telecentric lens system has been set up in order to improve accuracy and to avoid the 3D effects arising from using conventional entocentric lenses. The design of the telecentric lens system is discussed and reported along with an analysis of the spatial resolution of a BOS system using such kind of lenses. By neglecting lens aberration, the optimized telecentric BOS system has a spatial resolution which depends only on the schlieren object to background distance and on light wavelength, while optimum aperture results to linearly increase with the focal length of the frontal lens.

Based on the described optical design a double telecentric optical system was assembled and tested. The lens system showed good telecentricity, with a magnification changing of less than 0.2 % when the object is displaced of +/-20 mm respect to the sharp focus position.

A formula to relate the measured displacements and the integrated density gradient is inferred for the telecentric optical set-up. To correctly evaluate both the sensitivity of the BOS technique and the angular deflection of the light rays, the schlieren object to background distance has to be properly estimated. To this aim a method to estimate $Z_d$ based on ray-tracing that takes into account the presence of different refractive media is also described.

Finally the telecentric BOS system is used to analyze the supersonic flow outside a convergent-divergent nozzle operating under over-expanded conditions. The analysis of BOS images based on a cross-correlation algorithm allowed to visualize the shock structures and shear layers occurring in the transparent flow fields. For all the investigated cases information about the slopes of the shock waves and shear layers inferred from the measured virtual displacements showed a very good agreement with those evaluated from the tables of oblique shock.

The results confirmed that the designed telecentric lens is suitable for use in a BOS system, while further tests are required to quantitatively assess the improvement achievable in measuring plane 2D density field with telecentric imaging as compared to entocentric ones.

## Acknowledgments

This research is supported by ERC Consolidator Grant N. 617603, Project NSHOCK, funded under the FP7-IDEAS-ERC scheme. The authors would also like to thank OSRAM SpA Opto Semiconductors to have provided the high power LEDs and particularly Mr. Gabriele Giaffreda for his kindly assistance.

## References

[1] Schardin H 1942 Die Schlierenverfahren und ihre anwendungen *Ergebnisse der exakten Naturwissenschaften* 303
[2] Meier G E A 2000 Hintergrund Schlierenmessverfahren *German Patent, DE 199 42 856 A1*
[3] Raffel M, Richard H and Meier G E A 2000 On the applicability of background oriented optical tomography for large scale aerodynamic investigations *Exp. Fluids* **28** 477–81
[4] Elsinga G E, Van Oudheusden B W, Scarano F and Watt D W 2004 Assessment and application of quantitative schlieren methods: Calibrated color schlieren and background oriented schlieren *Exp. Fluids* **36** 309–25

[5] Venkatakrishnan L and Meier G E a. 2004 Density measurements using the Background Oriented Schlieren technique *Exp. Fluids* **37** 237–47
[6] Raffel M 2015 Background-oriented schlieren (BOS) techniques *Exp. Fluids* **56** 1–17
[7] Clem M M, Zaman K B M Q, Fagan A F and Glenn N 2012 Background Oriented Schlieren Applied to Study Shock Spacing in a Screeching Circular Jet *50th AIAA Aerosp. Sci. Meet.* 1–12
[8] Kindler K, Goldhahn E, Leopold F and Raffel M 2007 Recent developments in background oriented Schlieren methods for rotor blade tip vortex measurements *Exp. Fluids* **43** 233–40
[9] Bauknecht A, Merz C B, Landolt A, Meier A H and Raffel M 2013 Blade tip vortex detection in maneuvering flight using the Background Oriented Schlieren (BOS) technique *AHS 69th Annu. Forum Technol. Disp. "Advancing Vert. Flight Technol. Demanding Environ.* 1–13
[10] Cozzi F, Colombo L P M, Lucchini A, Coghe A, Muzzio A, Pacini F 2010 Background oriented schlieren characterization of the thermal boundary layer over a vertical heated plate in free convection *XVIII AIVELA National Meeting* (Rome) p 6
[11] Richard H and Raffel M 2001 Principle and applications of the background oriented schlieren (BOS) method *Meas. Sci. Technol.* **12** 1576–85
[12] Klinge F, Kirmse T and Kompenhans J 2003 Application of Quantitative Background Oriented Schlieren (BOS): Investigation of a Wing Tip Vortex in a Transonic Wind Tunnel *Proc. PSFVIP4* 1–11
[13] Goldhahn E and Seume J 2007 The background oriented schlieren technique: Sensitivity, accuracy, resolution and application to a three-dimensional density field *Exp. Fluids* **43** 241–9
[14] Venkatakrishnan L and Suriyanarayanan P 2009 Density field of supersonic separated flow past an afterbody nozzle using tomographic reconstruction of BOS data *Exp. Fluids* **47** 463–73
[15] Hargather M J and Settles G S 2010 Natural-background-oriented schlieren imaging *Exp. Fluids* **48** 59–68
[16] Konrath R and Schröder W 2002 Telecentric lenses for imaging in particle image velocimetry: a new stereoscopic approach *Exp. Fluids* **33** 703–8
[17] Born M and Wolf E 1999 *Principles of optics: Electromagnetic Theory of Propagation, Interference and Diffraction of Light* (Cambridge, New York: Cambridge University Press)
[18] Ota M, Leopold F, Noda R M K 2015 Improvement in spatial resolution of background-oriented schlieren technique by introducing a telecentric optical system and its application to supersonic flow *Exp. Fluids* **56** 48
[19] Vasil′ ev L A 1971 *Schlieren methods* (New York: Israel Program for Scientific Translations)
[20] Atcheson B, Heidrich W and Ihrke I 2009 An evaluation of optical flow algorithms for background oriented schlieren imaging *Exp. Fluids* **46** 467–76
[21] Raffel M, Willert C and Kompenhans J 2007 *Particle Image Velocimetry* (Berlin, Heidelberg: Springer Berlin Heidelberg)
[22] Merzkirch W 1987 *Flow visualization* (Orlando, Florida: Academic Press, Inc.)
[23] Berger C 2002 Design of telecentric imaging systems for noncontact velocity sensors *Opt. Eng.* **41** 2599
[24] Gojani A B, Kamishi B and Obayashi S 2013 Measurement sensitivity and resolution for background oriented schlieren during image recording *J. Vis.* **16** 201–7
[25] Gaskill J D 1978 *Linear systems, Fourier transforms, and optics." Linear Systems, Fourier Transforms, and Optics* (New York: John Wiley and Sons)
[26] Lagae A, Lefebvre S, Drettakis G and Dutré P 2009 Procedural noise using sparse Gabor convolution *ACM Trans. Graph.* **28** 1
[27] Adrian R J and Westerweel J 2011 *Particle Image Velocimetry*
[28] Thompson P A 1972 *Compressible-fluid dynamics* (New York: McGraw-Hill)